A medium-throughput crystallization approach

Gerlind Sulzenbacher, Arnaud Gruez, Véronique Roig-Zamboni, Silvia Spinelli, Christel Valencia, Fabienne Pagot, Renaud Vincentelli, Christophe Bignon, Aurelia Salomoni, Sacha Grisel, et al.

electronic reprint

A medium-throughput crystallization approach

Gerlind Sulzenbacher, Arnaud Gruez, Véronique Roig-Zamboni, Silvia Spinelli, Christel Valencia, Fabienne Pagot, Renaud Vincentelli, Christophe Bignon, Aurelia Salomoni, Sacha Grisel, Damien Maurin, Céline Huyghe, Kent Johansson, Alice Grassick, Alain Roussel, Yves Bourne, Sophie Perrier, Linda Miallau, Phillippe Cantau, Eric Blanc, Michel Genevois, Alain Grossi, André Zenatti, Valérie Campanacci and Christian Cambillau

A medium-throughput crystallization approach

Gerlind Sulzenbacher,[a]† Arnaud Gruez,[a]† Véronique Roig-Zamboni,[a]† Silvia Spinelli,[a]† Christel Valencia,[a] Fabienne Pagot,[a] Renaud Vincentelli,[a] Christophe Bignon,[a] Aurelia Salomoni,[a] Sacha Grisel,[a] Damien Maurin,[a] Céline Huyghe,[a] Kent Johansson,[a] Alice Grassick,[a] Alain Roussel,[a] Yves Bourne,[a] Sophie Perrier,[a] Linda Miallau,[a] Phillippe Cantau,[a] Eric Blanc,[a] Michel Genevois,[b] Alain Grossi,[b] André Zenatti,[b] Valérie Campanacci[a] and Christian Cambillau[a]*

[a]AFMB, UMR 6098, CNRS and Universités Aix-Marseille I and II, 31 Chemin J. Aiguier, F-13402 Marseille CEDEX 20, France, and [b]IBSM, IFR 88 CNRS, 31 Chemin J. Aiguier, F-13402 Marseille CEDEX 20, France

† These authors contributed equally to this work.

Correspondence e-mail:
cambillau@afmb.cnrs-mrs.fr

The first results of a medium-scale structural genomics program clearly demonstrate the value of using a medium-throughput crystallization approach based on a two-step procedure: a large screening step employing robotics, followed by manual or automated optimization of the crystallization conditions. The structural genomics program was based on cloning in the Gateway® vectors pDEST17, introducing a long 21-residue tail at the N-terminus. So far, this tail has not appeared to hamper crystallization. In ten months, 25 proteins were subjected to crystallization; 13 yielded crystals, of which ten led to usable data sets and five to structures. Furthermore, the results using a robot dispensing 50–200 nl drops indicate that smaller protein samples can be used for crystallization. These still partial results might indicate present and future directions for those who have to make crucial choices concerning their crystallization platform in structural genomics programs.

1. Introduction

Large-scale structural genomics programs, mainly initiated in the USA, rely deeply on automated methods for crystallization, crystal visualization and handling (Erlandsen *et al.*, 2000; Nienaber *et al.*, 2000; Thornton, 2001; Taylor, 2002). However, most of the present programs, publicly or privately funded, are set up on a scale out of reach for most European groups (Heinemann, 2000). A crucial issue is indeed to adapt the progress achieved in those large programs to smaller scale initiatives or to targeted projects.

Focusing on the crystallization steps only, three topics have been addressed: how to automize, parallelize and miniaturize crystallization. Automation itself was achieved a few years ago by robots using batch or vapour-diffusion technologies (Morris *et al.*, 1989). Current technologies, however, use smaller but denser plates; for example, the Greiner crystallization plates (Mueller *et al.*, 2001), with 96 reservoir wells and 288 sitting-drop shelves. New 384-well plates should become available soon. These plates are designed for the sitting-drop vapour-diffusion method and are well suited for parallelization through multi-needle dispensing robots. To date, all the classical approaches, automated or not, make use of crystallization drops with volumes ~1 µl. Companies or structural genomics consortia reported tremendous achievements in using a crystallization drop volume of a few tens of nanolitres, thus decreasing the amount of protein needed for crystallization by at least a factor of ten. Such improvements make it possible to use protein samples produced by low-volume cell-free expression systems (Alimov *et al.*, 2000;

Kigawa *et al.*, 1999), susceptible to yielding between 0.5–5 mg of protein, a quantity which would be sufficient for a complete crystallization experiment.

In this paper, we report preliminary crystallization results of a medium-scale structural genomics program aiming to solve the three-dimensional structures of 110 *Escherichia coli* targets of unknown function, in which easier and faster cloning and protein production was based on the Gateway® system (Walhout *et al.*, 2000). ORFs of unknown function but common to two or several other bacteria have been chosen. Extensive use of a new generation of crystallization robots has been followed by automated or manual refinement of crystallization conditions and experiments with nanocrystallization technology. The proteins bore a 21-residue-long N-terminal tail comprising a His$_6$ tag and a linker present in the Gateway® pDEST17 plasmid (Walhout *et al.*, 2000). The presence of this extension indeed raised questions about the ability of the recombinant proteins to crystallize. A clear answer to this question has been obtained since 13 proteins (out of 25 purified) yielded crystals in 20 different crystal forms.
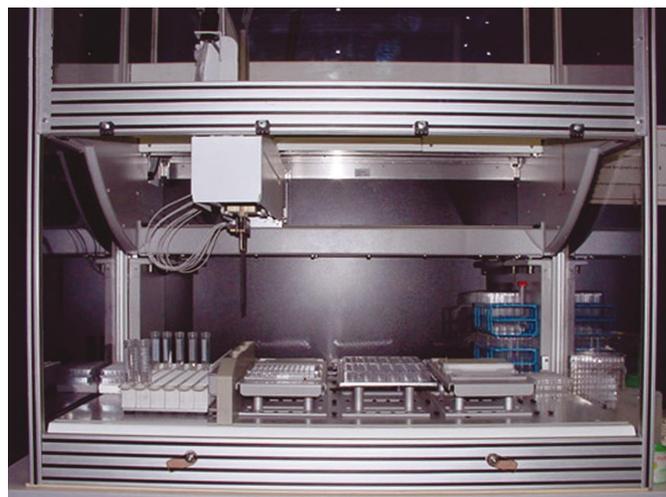
2. Material and methods

2.1. Protein production

The production and purification of the 110 *E. coli* ORFs will be reported elsewhere. In brief, the ORFs were subcloned in the Gateway® system (Invitrogen, pDEST17 plasmid) introducing 15 amino acids plus six histidines at the N-terminus (Walhout *et al.*, 2000). Expression of proteins was performed using eight different *E. coli* strains as described by Vincentelli *et al.* (2002). Purification was performed on a Pharmacia Äkta FPLC with an IMAC column, followed by preparative gel filtration. The proteins were characterized by SDS–PAGE, mass spectroscopy (Leushner, 2001), circular dichroism (van Mierlo & Steensma, 2000) and dynamic light scattering (DLS; Bernstein *et al.*, 1998).

2.2. Robotics setup for screening with commercial kits

Crystallization experiments were performed immediately after protein purification. Screening experiments were performed with several commercial kits: Structure Screens 1 and 2 (Jancarik & Kim, 1991), Clear Strategy Screens 1 and 2 (Brzozowski & Walton, 2001), ZetaSol (Riès-Kautt & Ducruix, 1997), Stura Footprint Screen (Stura *et al.*, 1992) (Molecular Dimensions Limited, http://www.moleculardimensions.com/) and Wizard Screens I and II (Emerald BioStructures, http://www.emeraldbiostructures.com).

(a)

(b)

Figure 2
Views of the modifications applied to the Genesis Robot. (*a*) The closed cabinet preventing evaporation; (*b*) the tube-holder tray.
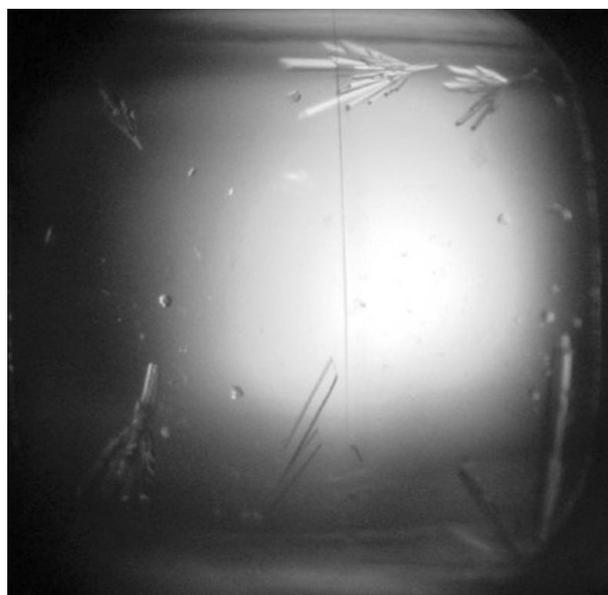
Figure 1
An example of a Greiner plate lateral sitting-drop shelf filled with 1.5 µl protein and 1.5 µl precipitant solution. The shelf is completely filled and crystals are therefore well visualized, even at the edges.

The screens were set up in 8 × 12 well Greiner crystallization plates, with three shelves for each well (reference numbers 609160 or 609120; Friekenhausen, Germany) and each condition was tested at three different protein concentrations, yielding a total of 1272 crystallization drops and consuming ~10–20 mg of protein. Reservoir solutions were 200 µl in volume and crystallization drops were composed of 1–1.5 µl protein solution and an equal amount of reservoir solution (Fig. 1).

The drops were set up in parallel mode using a TECAN Genesis robot with eight low-volume needles. Reservoir and protein solutions were mixed after dispensing in order to avoid effects of local supersaturation. For a better control of humidity, the robot was mounted in a closed cabinet in a room at 293 K (Fig. 2a). The tubes containing the crystallization solutions were placed on a tube-holder plate, modified such that the tubes could be opened readily (Fig. 2b). Although the *GEMINI* software driving the TECAN robot allows fine-tuning of liquid-handling parameters for individual solutions (fluid *versus* viscous *etc.*), the same parameters, adjusted on the most viscous solution, were used for the handling of all solutions. The screening strategy was optimized such that crystallization plates were filled with reservoir solutions beforehand, in order to be ready for crystallization drop setup without delay. The crystallization plates were sealed with transparent film after set-up of the drops and transferred to a storage cabinet at 293 K.

2.3. Crystal improvement

The crystallization plates containing the first screening experiments were regularly observed in a standard way. As soon as preliminary hints became available, improvement of crystallization conditions was carried out either by traditional methods or employing solutions from an optimization matrix dispensed by robots. In the former case, the optimization experiments made use of the hanging-drop vapour-diffusion method and were set up by hand in 24-well plates. These plates were greased automatically by a crystallization robot build in-house. Automated crystal optimization was carried out by varying two parameters at a time (*e.g.* pH and precipitant concentration), exploring the parameter space around the initial conditions identified during the screening step. Matrices of 8 × 8 conditions were established and varying amounts of four stock solutions were distributed and subsequently mixed by the TECAN robot within 64 wells of the Greiner plates. These plates were subsequently used for microlitre or nano-litre crystallization.

2.4. Nanolitre crystallization

The nanolitre crystallization experiments were performed using the sitting-drop method in the Greiner plates. As mentioned above, for each commercial screen condition, three protein concentrations were used, yielding a total of 1272 crystallization drops if all screens were used. The reservoirs of the Greiner plates were filled up using the TECAN robot, while the nanolitre drops were dispensed by a Cartesian robot

(Fig. 3a). The Cartesian robot, controlled by the *AXSYS* software, is contained in a closed cabinet in order to control the humidity level and avoid evaporation of the drops. The humidity level is kept at 85–90%. The dispense head holds eight high-speed microsolenoid valves with their respective low-volume ceramic tips (Fig. 3b). The rate of aspiration and dispensation of the crystallization buffers depends on the solvent properties (concentration and viscosity). It was adjusted for handling the most viscous solutions of concentrated high-molecular-weight PEGs (30% PEG 8000, 30% PEG 10 000). An air gap of 4 µl prevented the dilution of the working solution by the system fluid (water). After aspiration

(a)

(b)
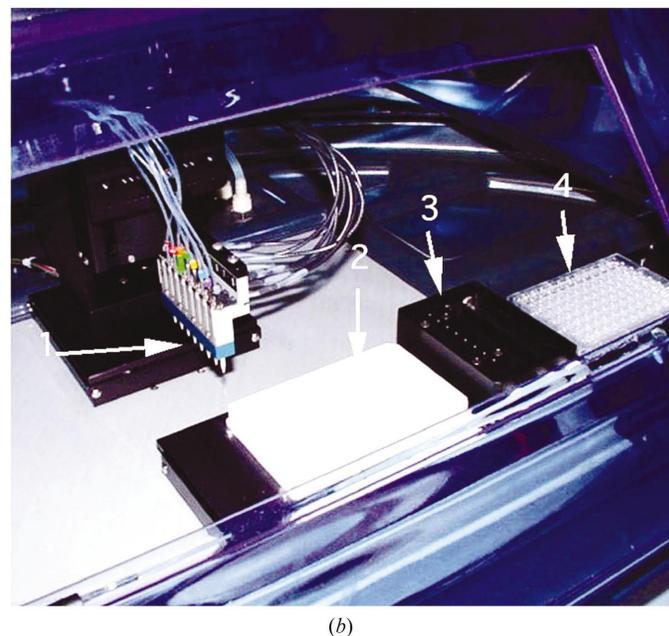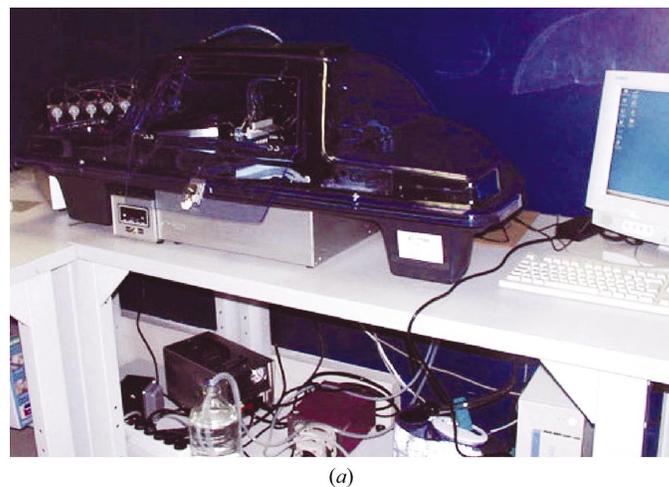
Figure 3
The nanodrops dispensing robot (Cartesian Inc.) (a) The carriage and the dispensing tips are contained in a closed box and the humidity is maintained at 85–90%. (b) The setting used for crystallization: the eight tips (1) aspirate the protein in the 28 µl wells of a 16 × 24 plate (2) and dispense it on the sitting-drop shelves of the 96 wells of the Greiner plate (4). The operation can be repeated for three proteins or for the same protein at three different concentrations. For aspiration and dispensing precipitant solutions, the eight tips are used and washed in the 'wash station' (3) between pipetting of each row.

Table 1
Diffraction data.

Values in parentheses are for the highest resolution shell.

Data	Target 12	Target 28	Target 30	Target 45	Target 56	Target 57a	Target 65a	Target 87	Target 104	Target 112
Beamline	ID14-EH1	Rigaku/MAR 345 dtb	ID14-EH2	ID14-EH1	ID14-EH1	Rigaku	ID14-EH1	ID14-EH1	BM14	ID14-EH1
Temperature (K)	100	100	100	100	100	100	100	100	100	100
Wavelength (Å)	0.934	1.5418	0.933	0.954	0.934	1.54179	0.934	0.934	0.950	0.934
No. of images	203	174	768	158	120	172	90	200	220	90
Oscillation per frame (°)	1	1	0.5	1	1	1	1	1.0	0.5	1
Space group	$C2$	$P2_1$	$P2_1$	$C222_1$	$P4_322$	$P2$	$P3$	$P2_1$	$P2_12_12_1$	$P2_12_12_1$
Unit-cell parameters										
a (Å)	115.92	85.03	85.04	142.3	55.4	62.29	83.5	80.5	61.27	58.0
b (Å)	39.30	79.68	79.68	144.9	55.4	103.68	83.5	56.6	118.68	81.5
c (Å)	69.15	158.66	158.66	166.3	196.6	108.56	188.3	148.8	136.48	89.8
α (°)	90.00	90.00	90.00	90	90.00	90.0	90	90	90.00	90
β (°)	116.19	101.7	95.76	90	90.00	104.80	90	101.7	90.00	90
γ (°)	90.00	90.00	90.00	90	90.00	90.0	90	90	90.00	90
No. of monomers per a.u.	1	4	4	4	1	1	2	4	2	2
Resolution range (Å)	25.0–1.50 (1.58–1.50)	20.0–2.0 (2.08–2.0)	20–2.0 (2.07–2.0)	45–2.35 (2.48–2.35)	20–2.25 (2.31–2.25)	20–2.54 (2.61–2.54)	25–2.2	20.0–2.5 (2.54–2.5)	20–1.64 (1.7–1.64)	27–1.8
No. of observations	164575	258562 (18117)	797404	70214	15661	36410	303556	170923	397033	132263
Unique reflections	43648	70083 (5721)	137248	353959	134857	109009	58358	45683	86801	37692
Redundancy	3.7 (3.5)	3.5 (3.2)	5.8 (1.9)	5.0 (4.7)	8.6 (8.9)	3.0 (3.0)	5.2 (5.0)	3.9 (3.9)	4.0 (2.0)	3.4 (3.0)
Completeness (%)	99.4 (99.4)	96.6 (96.6)	96.3 (96.3)	99.7 (99.7)	99.1 (99.1)	82.4 (82.4)	99.9 (99.8)	99.3 (99.3)	96.9 (79.6)	99.4 (99.4)
$I/\sigma(I)$	7.6 (2.5)	11 (3.6)	7.1 (3.6)	3.5 (2.2)	11.7 (1.8)	7.0 (2.0)	7.5 (2.5)	11.0 (5.2)	10.4 (2.30)	6.6 (2.0)
R_{sym}† (%)	5.7 (28.3)	6.1 (24)	7.6 (19.8)	7.4 (31.7)	4.6 (42.5)	7.8 (38)	6.1 (32.5)	4.6 (3.3)	4.7 (32.7)	6.8 (28.5)

† $R_{sym} = \sum_h \sum_i [I_{(h,I)} - \langle I \rangle_h] / \sum_h \sum_i \langle I \rangle_h$.

of the solutions, the pressure in the tubing system increased, and in order to be able to dispense nanolitre volumes with accuracy, the pressure needed to be brought back to a lower value. This was performed by a pre-dispense step of 0.6 µl.

Low volumes of protein samples were aspirated by eight tips in parallel and for each well of the 8 × 12 Greiner plates
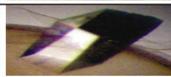
volumes of 50–200 nl were dispensed on the leftmost of three sitting-drop shelves (see Fig. 4). This procedure was repeated in order to fill the three shelves with three different protein concentrations, or, in special cases, with three different proteins. Subsequently, the triple amount of 50–100 nl of the reservoir solutions were aspirated by the eight tips and added to the three protein drops. This operation was repeated 12 times until the eight rows were complete. Finally, the plates were sealed with a transparent film and stored in a cabinet at 293 K.
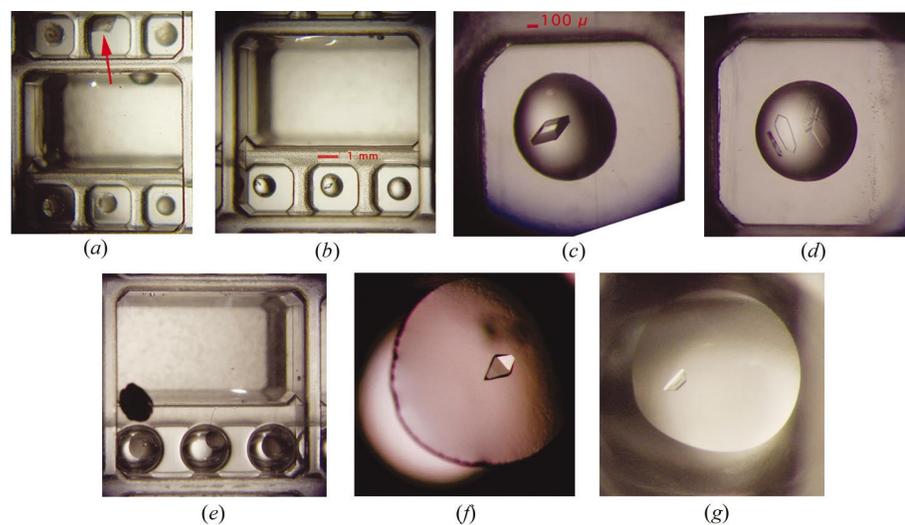
Figure 4
Crystallization with 100 nl drops. (*a*) One of the 96 wells of the Greiner 'flat-bottom' crystallization plate. The large main well contains the precipitant solution and the three small lateral shelves contain the crystallization drops (here, 100 nl after vapour equilibrium is reached). Note that the drop in the second shelf is localized at the edge (red arrow); (*b*) One of the 96 wells with a lysozyme crystal in the crystallization shelf; (*c*) close-up view of the crystal from (*b*). Its size (∼0.35 × 0.1 × 0.1 mm) is appropriate for synchrotron data collection. (*d*) Long flat crystals of target 87. (*e*) One of the 96 wells of the Greiner 'round-bottom' crystallization plate. (*f*) and (*g*), crystals formed in the 'round-bottom' crystallization shelves.

2.5. Dynamic light scattering

DLS analyses were carried out with a Dynapro-MS800 instrument (Protein Solutions). Before measurement, the proteins were filtered with a Millipore 4 mm syringe unit. The measurements were performed by injecting 15 µl of protein buffered with Tris–HCl 20 mM pH 7.8 at ∼2 mg ml^{-1}. All calculations were carried out using the software provided with the instrument. Four independent measurements of 20 acquisitions were carried out for each protein. Apparent molecular masses were deduced from the measurements (Fig. 5).

Target No.	tMW (kDa)	aMW (kDa)	Cp (%)	Initial crystallization screening conditions	Final crystallization conditions	Picture
12	36	30 ± 2 ×1	16	None	13% PEG 4K, 2% MPD, 0.05 M Na cacodylate pH 6.2	
28a	34	103 ± 3 ×3	13	**MDL I-5**: 2 M $(NH_4)_2SO_4$, 0.1 M Na acetate pH4.6	2 M $(NH_4)_2SO_4$, 5% dioxane, 0.1 M Na acetate pH 5.0	
28b				**Stura I A-1**: 15% PEG 600, 0.2 M imidazole-malate pH 5.5	None	
28c				**MDL II-23**: 1.6 M $(NH_4)_2SO_4$, 10% dioxane, 0.1 M MES pH 6.5	2.1 M $(NH_4)_2SO_4$, 5 % dioxane, 0.1 M Na acetate pH 5.5	
30a	53	N/D		**Wizard II-36**: 10% PEG 3K, 0.2 M NaCl, 0.1 M phosphate–citrate pH 4.2	8% PEG 3350, 0.2 M NaCl, 0.1 M phosphate–citrate pH 4.5	
30b				**Stura II-B4**: 15% PEG 4K, 0.1 M imidazole–malate pH 6.0	7% PEG 4K, 0.1 M imidazole–malate pH 6.0	
33a	38	113 ± 4 390 ± 40 ×?	9 42	**MDL I-31**: 20% PEG 4K, 10% isopropanol, 0.1 M HEPES pH 7.5	12% PEG 4K, 10% isopropanol, 0.1 M HEPES pH 7.5	
33b				**MDL I-7**: 30% PEG 4K, 0.2 M ammonium acetate, 0.1 M Na citrate pH 5.6	20% PEG 4K, 0.1 M ammonium acetate, 0.1 M Na citrate pH5.5	
45	34	95± 12 (76 ± 0) ×2/×3?	18 (18)	**Wizard II-8**: 10% PEG 8K, 0.2 M NaCl, 0.1 M Na/K phosphate pH 6.2	8% PEG 10K, 0.2 M NaCl, 0.2 M imidazole–malate pH 5.8	
56	37	78 ± 2 86 ± 1 ×2	18 12	**Stura II-D1**: 42% PEG 600, 0.2 M imidazole–malate pH 5.5	39% PEG 600, 0.1 M HEPES pH 7.5	
57a	45	80 ± 0; (77 ± 0) ×2	14 (18)	**Stura II-C3**: 36% MPEG 2K, 0.1 M Na cacodylate pH 6.5	None	
57b				**Stura I-B6**: 1 M Na citrate, 0.01 M Na borate pH 8.5	0.9 M Na citrate, 0.01 M Na borate pH 8.5	
65a	41	85 ± 1; 160 ± 35; (127 ± 33) ×2 or ×4	23, 24 (23)	**Stura II-D2**: 45% PEG 600, 0.1 M HEPES pH 7.5	42% PEG 600, 0.1 M HEPES pH 7.5	
65b				**Stura II-A5**: 8% MPEG 5K, 0.2 M imidazole–malate pH 5.5	10% MPEG 5K, 0.2 M imidazole–malate pH 5.5	
73a	63	162 ± 5 ×2/×3?	23	**Stura I-A4**: 0.75 M $(NH_4)_2SO_4$, 0.15 M Na citrate pH 5.5	0.8 M $(NH_4)_2SO_4$, 0.15 M Na citrate pH5.5	
73b				**MDL I-12**: 1.4 M Na acetate, 0.1 M Na cacodylate pH 6.5	1.2 M Na acetate, 0.1 M Na cacodylate pH 6.5	
87	35	95 ± 3 (60 ± 5) ×2?	23 (12)	**Stura II-B1**: 18% PEG 600, 0.1 M HEPES pH 7.5	11% PEG 600, 0.1 M imidazole–malate pH 6.5	
91	44	98 ± 7 105 ± 26 ×2	10 14	**Wizard I-40**: 10% isopropanol, 0.2 M $Ca(OAc)_2$, 0.1 M MES pH 6.0	13% isopropanol, 0.2 M $Ca(OAc)_2$, 0.1 M MES pH 6.0	
104	48	85 ± 10 (90 ± 25) ×2	24 (23)	**MDL I-10**: 0.1 M $(NH_4)H_2PO_4$, 0.1 M Na citrate pH 5.6	0.9 M $(NH_4)H_2PO_4$, 0.1 M HEPES pH 7.0	
110	20	20 ± 1 (26 ± 1) ×1	14 (8)	**Stura I-A6**: 0.75 M Na citrate, 0.01 M Na borate pH 8.5	0.7 M Na citrate, 0.05 M Na borate pH 7.0	
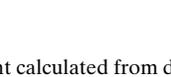
Figure 5
Dynamic light-scattering and crystallization results. tMW: theoretical molecular weight. aMW: apparent molecular weight calculated from dynamic light-scattering data ± estimated error; different values refer to measurements taken on different samples; values in parentheses refer to selenomethionylated samples; ×1: monomer; ×2: dimer; ×4: tetramer. Cp: polydispersity. Cp < 15% R_H, negligible polydispersity; Cp < 30% R_H, moderate amount of polydispersity; CP > 30% R_H, significant amount of polydispersity. N/D, not determined.

2.6. Cryocooling and data collection

All data sets were collected at 100 K on flash-frozen crystals. Each crystal required specific cryocooling conditions, which were adjusted by adding varying amounts of glycerol, ethylene glycol or low molecular-weight PEGs to the crystallization cocktail. The crystals were collected using commercial cryo-loops (Hampton Research) and flash-cooled in an N_2 stream at 100 K. Data were collected either at the European Synchrotron Radiation Facility (ESRF, Grenoble) or in-house using a Cu rotating-anode generator with OSMIC mirrors and MAR Research imaging plates. Data were indexed and integrated with the programs *DENZO* (Otwinowski & Minor, 1997) and *SCALA* (Collaborative Computational Project, Number 4, 1994). Data-collection statistics are summarized in Table 1. The structures were solved by SAD or MAD experiments at the Se edge (Hendrickson, 1991), performed at ESRF (Grenoble), using SeMet-substituted proteins produced by the methionine-pathway inhibition method (Doublie, 1997).

3. Results and discussion

3.1. Crystallization

The crystallization experiments were performed in a sequential way: in a first step, or when protein quantity was scarce, three screens were used, providing 244 different conditions: Stura Footprint Screen, Wizard I and II and Structure Screens 1 and 2. When protein supply was abundant or when crystallization failed, a second step was performed involving the Clear and ZetaSol screens, thus bringing the experiments to a total of 424 conditions.

Eleven months after the start of the project, a total of 25 soluble proteins were brought to crystallization and 13 crystallized (Fig. 4). This crystallization success (55%) indicates first that the long 21-amino-acid tail does not prevent the proteins from crystallizing. Indeed, its influence on the crystal quality is not yet documented. As indicated in Fig. 4, the 13 crystallized proteins yielded macroscopic crystals in 20 different crystal forms: seven gave a unique crystal form, five gave two crystal forms and one gave three crystal forms. When different crystal forms were obtained for the same native protein (targets 28, 30, 33, 57, 65 and 73), they originated from different conditions. Some proteins crystallized also with cofactors, leading in some cases to new crystal forms (data not shown). In all cases but one (target 12) the first crystals were obtained with crystallization conditions from the commercial kits (Fig. 5). However, crystal optimization was necessary to obtain well shaped and diffracting crystals, with the exceptions of targets 28b and 57a. All kits did not have the same success ratio, although all were not used to the same extent. The most successful kits were, indeed, those used in the first crystallization step. The 'Stura' kit proved to be by far the most efficient, providing crystals for eight proteins out of 13 (61%) and ten crystal forms out of 20 (50%). The Structure Screen kit yielded six crystal forms and the Wizard kit three. The Clear and the ZetaSol kits did not yield any crystals in the second crystallization step.

3.2. Dynamic light scattering (DLS)

DLS did not identify aggregation in any of the proteins which crystallized. In some cases, the experiments clearly indicated the monomeric/oligomeric nature of the protein in the buffer solution. Targets 12 and 110 are clearly monomeric, while targets 56, 57, 91 and 104 are dimeric. However, some differences have been observed between different batches, as for example with targets 33 and 65, or between the native and SeMet-labelled protein (targets 45, 65, 87). Since the measurement conditions were very similar for different batches, it should be considered that minor modifications on protein concentration, pH or buffer composition might drastically affect the DLS results.

3.3. Diffraction data

Preliminary diffraction data were always collected on a rotating-anode generator prior to synchrotron data collection. Crystals from selenomethionine-labelled protein were brought to the synchrotron after collecting data on the native crystals. A total of ten native data sets were collected. Considering the resolution in shells of 0.5 Å, one crystal (target 12) diffracted to 1.5 Å, two crystals (targets 104 and 112) diffracted to 1.5–2.0 Å, five crystals to 2.0–2.5 Å (targets 28, 30, 56, 65, 87) and two crystals diffracted to less than 2.5 Å resolution. R_{sym} values range between 4 and 8%.

3.4. Nanolitre crystallization

The Cartesian dispensing robot uses high-speed micro-solenoid valves and is able to dispense 'on-the-fly' drops as small as 10 nl (Fig. 4). This allows crystallization experiments to be performed with a reduced amount of material compared with the traditional approaches. As an example, 100 µl of protein solution (1 mg of protein at 10 mg ml^{-1}) is sufficient to generate 1000 drops of 100 nl with different conditions.

Our first aim was to reproduce rod-shaped lysozyme crystals. The drops were set up using a protein concentration half of that of the reported procedure, using 200 nl of protein solution mixed with 100 nl of precipitant (1.2 *M* sodium chloride in 100 m*M* acetate buffer pH 4.6) (Fig. 4*c*). Some drops, however, slipped to the shelf edge, rendering the observation of crystals difficult (Fig. 4*a*). This problem could partly be overcome by diminishing the drop size. The definitive solution was obtained with 'round-bottom' Greiner crystallization plates (reference number 609120) in which the shelf shape is spherical (Figs. 4*e*–4*g*), at the expense of a less clear visualization of the drop. Good well shaped lysozyme crystals were obtained readily, with kinetics faster than with the 1 µl drops. Crystals appeared within 4 h and, under these conditions, 50% of the drops contained nicely formed crystals (Fig. 4*b*), while the second half contained crystals as well as clusters of needles. Additional crystallization experiments were performed with two other proteins (targets 28 and 87), which demonstrated that it is possible to obtain new and different crystal forms in the same small drop (Fig. 4*c*). Our first experiments indicate clearly that the nanodrop technology yields more crystal forms than classical crystallization, manual

or not. This might be a consequence of the faster equilibration rate preventing protein degradation or skin formation at the drop surface. The nanodrop dispensing robot is now used routinely.

4. Conclusions

The Gateway^{TM} technology, which makes it possible to clone rapidly with near 100% efficiency, introduces a 21-amino-acid tail. Our experiments indicated that this tail does not prevent crystallization and that the crystal quality is comparable with that obtained from standard procedures. Our first results indicate that of the various commercial kits, the Stura Foot-print Screen proved to be the most efficient in producing crystals. A selection or redesign of commercial kits might therefore become necessary in order to save protein material when it is scarce. The benefit of nanotechnologies is apparent when considering protein economy. Furthermore, the crystallization conditions are comparable with those found with higher volumes, indicating that reproducibility will not become a problem. It is therefore possible to routinely obtain crystals within hours, instead of days, by employing nano-technologies.

References

Alimov, A. P., Khmelnitsky, A. Y., Simonenko, P. N., Spirin, A. S. & Chetverin, A. B. (2000). *Biotechniques*, **28**, 338–344.

Bernstein, B. E., Michels, P. A., Kim, H., Petra, P. H. & Hol, W. G. (1998). *Protein Sci.* **7**, 504–507.

Brzozowski, A. M. & Walton, J. (2001). *J. Appl. Cryst.* **34**, 97–101.

Collaborative Computational Project, Number 4 (1994). *Acta Cryst.* D**50**, 760–763.

Doublie, S. (1997). *Methods Enzymol.* **276**, 523–530.

Erlandsen, H., Abola, E. E. & Stevens, R. C. (2000). *Curr. Opin. Struct. Biol.* **10**, 719–730.

Heinemann, U. (2000). *Nature Struct. Biol.* **7**(*Suppl.*), 940–942.

Hendrickson, W. A. (1991). *Science*, **254**, 51–58.

Jancarik, J. & Kim, S.-H. (1991). *J. Appl. Cryst.* **24**, 409–411.

Kigawa, T., Yabuki, T., Yoshida, Y., Tsutsui, M., Ito, Y., Shibata, T. & Yokoyama, S. (1999). *FEBS Lett.* **442**, 15–19.

Leushner, J. (2001). *Expert Rev. Mol. Diagn.* **1**, 11–18.

Mierlo, C. P. van & Steensma, E. (2000). *J. Biotechnol.* **79**, 281–298.

Morris, D. W., Kim, C. Y. & McPherson, A. (1989). *Biotechniques*, **7**, 522–527.

Mueller, U., Nyarsik, L., Horn, M., Rauth, H., Przewieslik, T., Saenger, W., Lehrach, H. & Eickhoff, H. J. (2001). *Biotechnol.* **85**, 7–14.

Nienaber, V. L., Richardson, P. L., Klighofer, V., Bouska, J. J., Giranda, V. L. & Greer, J. (2000). *Nature Biotechnol.* **18**, 1105–1108.

Otwinowski, Z. & Minor, W. (1997). *Methods Enzymol.* **276**, 307–326.

Riès-Kautt, M. & Ducruix, A. (1997). *Methods Enzymol.* **276**, 23–59.

Stura, E. A., Nemerow, G. R. & Wilson, I. A. (1992). *J. Cryst. Growth*, **122**, 273–285.

Taylor, W. R. (2002). *Nature (London)*, **416**, 657–660.

Thornton, J. (2001). *Trends Biochem. Sci.* **26**, 88–90.

Vincentelli, R., Bignon, C., Gruez, A., Sulzenbacher, G., Tegoni, M., Campanacci, V. & Cambillau, C. (2002). Submitted.

Walhout, A. J., Temple, G. F., Brasch, M. A., Hartley, J. L., Lorson, M. A., van den Heuvel, S. & Vidal, M. (2000). *Methods Enzymol.* **328**, 575–592.